DOI: 10.13009/EUCASS2023-949
Aerospace Europe Conference 2023 – 10TH EUCASS – 9TH CEAS

Total Energy Control for the Automatic Landing of UAS with Large Aspect Ratio and Low Wing Loading

Bryan Laabs†, Robert Luckner*, Ralph Paul**, Nikolai Block**
* Technische Universität Berlin, Institut für Luft und Raumfahrttechnik, Marchstr. 12-14, 10587 Berlin, Germany
** Leichtwerk AG, Hermann-Blenk-Straße 38, 38108 Braunschweig, Germany
bryan.laabs@tu-berlin.de† - robert.luckner@tu-berlin.de - ralph.paul@fd-tec.net - nikolai.block@itk-engineering.de

Abstract

Automatic landing of unmanned, high-altitude long-endurance aircraft, characterized by large wingspans, very low wing loading and - here - by a tail-dragger configuration, requires control strategies that differ from classical Autoland systems. The paper describes an implementation based on Lambregts's Total Energy Control System concept to ensure accurate tracking of airspeed, pitch attitude, and sink rate throughout the specific flight phases during landing. This novel strategy requires an adaption of the control allocation prior to touchdown using continuous flap settings for vertical speed control. The performance of the design is demonstrated by an extensive Monte Carlo simulation.

1. Introduction

As an alternative to the increasing number of satellites in orbit, high-altitude long-endurance (HALE) aircraft (A/C) are under development to serve as unmanned high-altitude platform stations (HAPS), also called pseudo satellites, for aerial surveillance or as telecommunication hubs. To achieve long endurance for the intended missions, HAPS are designed as fixed-wing A/C with a large aspect ratio and very low wing loading (< 150 N/m^2). They are operated in the lower stratosphere, where environmental conditions allow for geostationary operations. Due to the risks associated with their size and their operation over populated areas, these HAPS A/C are classified in the certified category according to [1], for which certification authorities currently develop the certification rules. Even though the landing is a short phase of the intended mission, here the A/C can be exposed to severe turbulence and is operated in dense controlled airspace, where it has to comply to applicable approach procedures and consider surrounding traffic and terrain. As of today, no specific certification requirements for unmanned HAPS A/C are established. Therefore, the requirements for the Autoland function that are listed in Table 2 are derived from requirements for commercial air transport [2] and standards for fixed-wing UAS [3]. During the approach in full-automatic landing mode, the flight control laws (FCL) have to guide the A/C precisely along the glide path while maintaining the airspeed within tight boundaries. Furthermore, the FCL have to ensure that the A/C touches the ground at defined airspeed, vertical speed and pitch attitude as well as within a safe bank attitude range.
As a strategy to control the highly coupled airspeed and altitude dynamics of the A/C by an integrated controller, Lambregts invented the concept of the Total Energy Control System (TECS) [5], [6], [7]. TECS was flight tested first on a Boeing 737 [8] and used in the autopilot of the Boeing Condor UAV, a large aspect ratio UAV equipped with piston engines operating in the lower stratosphere. For the LAPAZ project at TU Berlin, the TECS concept was adapted for automatic landing (Autoland) of the high aspect ratio motor-glider Stemme S15 [11]. During the LAPAZ project, the TECS-based Autoland function was flight-tested for regular landings and glider landings [10],[12]. The concept of total energy control was successfully evaluated for HAPS A/C [13]. It is intended to be applied to the solar-powered high aspect-ratio HAP alpha A/C that DLR currently develops [14]. This paper describes the implementation of TECS to enable the fully automatic operation including the automatic landing of the HAPS A/C “StratoStreamer” which is in development at Leichtwerk AG (Section 2). In comparison to [10] and [12], the low wing loading and the intended three-point landing of this taildragger A/C pose novel design challenges for the Autoland function development. TU Berlin developed the flight control functions (FCF) for the “StratoStreamer” A/C in the research projects FCL-HALE and IBAS-TUB.
For FCF development using MATLAB and Simulink/Stateflow, a high-fidelity non-linear flight mechanical model of the A/C and linear models of the A/C motion are available at any trim point throughout the flight envelope. For the initial FCF gain sizing, linear methods in MATLAB are used. Implementing the FCF as flight control laws (FCL) in Simulink/Stateflow yields a so-called Prototype Model that is integrated into the non-linear simulation. The gains of the FCF are optimized using both linear and non-linear simulation results. The controller synthesis utilizes the DLR

DOI: 10.13009/EUCASS2023-949

multi-objective design tool MOPS (Multi-Objective Parameter Synthesis)[16]. Model-based development of the FCL Software (SW) including the Autoland function was conducted in compliance with RTCA DO-178C and DO-331. The Prototype Model is automatically translated into a Design Model in SCADE. By model-based testing in the research project IBAS-TUB, full decision coverage was achieved and comparable SW behaviour on desktop PCs and the target flight control computer was demonstrated [17].
Based on the "StratoStreamer" A/C (Section 2), the requirements for the Autoland function are identified in Section 3. Section 4 outlines the intended Autoland procedure in accordance with [4]. The FCF for control of the longitudinal A/C motion are organized in a TECS-based cascaded controller structure. The Autoland function for the taildragger A/C has to ensure precise control of pitch attitude, approach airspeed and sink rate prior to touchdown. For this control task, the classical TECS control allocation strategy is adapted over the runway and the flaps are continuously utilized for vertical speed control. The FCF for the lateral A/C motion are not discussed in this paper. Section 5 describes the FCF design process, the required adaptations of the classical TECS concept and the integration of the Autoland function into the chosen cascaded controller structure. The effectiveness of the design is demonstrated in Section 5. The reliability and robustness of the design against the derived certification requirements (Section 3) is demonstrated by an extensive Monte Carlo simulation in Section 6. Within the Monte Carlo simulation, MOPS [16] automatically determines the risk to exceed the specified limits of Table 2.

2. Description of the HAPS A/C "StratoStreamer"

Figure 1 shows the "StratoStreamer" HAPS A/C. It is equipped with conventional control surfaces: an elevator for pitch control, a rudder for yaw control and six flaperons on each half of the wing provide roll control as well as lift (see Figure 2). All aerodynamic control surfaces are actuated by electric actuators. The full fly-by-wire flight control system of the A/C does not contain any mechanical linkage between the control surfaces. The flaperons provide a flap function by biasing all flaperons by the same value. A speed brake function with pre-defined discrete settings is provided using the four inner flaperon pairs, whereupon the innermost flaperon pair deflects downwards to account for the reduced lift that is caused by the negative deflection of the other flaperon pairs. The mixing ratio that yields the individual flaperon deflection commands from the aileron function, the flap function and speed brake function is the result of aerodynamic analyses. The mixing function is realized in the FCL SW. The A/C is equipped with a pair of electric engines in a pusher configuration. The A/C is a taildragger that incorporates a swivel-mounted main landing gear and a tail wheel that is mechanically linked to the rudder for steering on ground. The A/C is designed for operations in the lower stratosphere at around FL600 [19]. However, this paper only focusses on operation close to the ground during the landing approach.

Figure 1: "StratoStreamer" HAPS A/C [20]

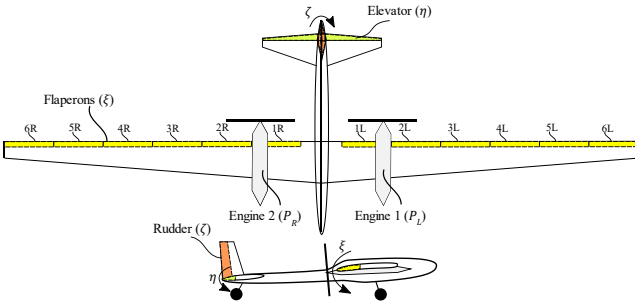

Figure 2: "StratoStreamer" Flight Controls

In contrast to other HAPS with a similar configuration such as the DLR HAP alpha [15], the A/C is powered by batteries and a hydrogen fuel cell. The advanced light weight construction techniques of Leichtwerk AG permit the assumption that the dynamics can be formulated as rigid-body dynamics. Differently from [14], it is assumed that the frequencies of the first aeroelastic modes of the A/C are significantly higher than the frequency of the short-period motion. Therefore, the aeroelastic effects are not considered. For FCF development, a high-fidelity 6-degrees of freedom (6DoF) non-linear flight mechanical model of the A/C is available. Linear approximations of the short-period motion or the full longitudinal motion can be generated by linearization at any trim point within the flight envelope. Figure 3 shows the poles of the short-period motion and the phugoid motion at ten trim points throughout the full airspeed range at flight level FL033 that are used for design of the FCF in Section 5. The short-period motion is highly damped yet still oscillatory in the overall airspeed range at damping ratios above $D > 0.95$. Close to the stall speed, the frequency of the short-period motion exceeds 3 rad/s. The frequency of the phugoid reduces over the airspeed range from around 0.3 rad/s to 0.15 rad/s whereas D remains > 0.2. Both the characteristics of the short-period motion and the phugoid do not pose any particular challenges to the control of the longitudinal motion. Frequency spacing between

DOI: 10.13009/EUCASS2023-949

the eigen motions allows for a classical cascaded controller design, e.g., with the pitch controller operating in the frequency range of the short-period motion and the flight path controller in the frequency range of the phugoid.

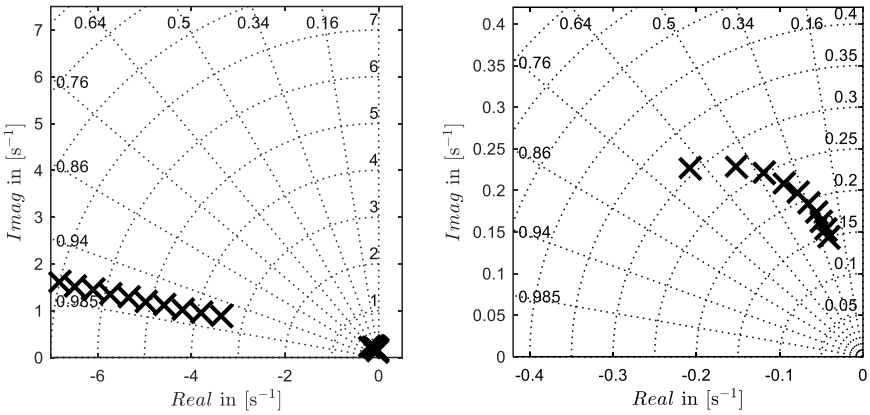

Figure 3: Poles of the short-period motion and phugoid at 3300 ft (left), poles of the phugoid (right)

3. Requirements for the Automatic Landing

As of today, no specific certification requirements for unmanned HAPS A/C are established. Table 2 lists the requirements for the Autoland function developed in the FCL research programme that are derived from comparable requirements for commercial air transport [2] and applicable standards for fixed-wing UAS [3]. These requirements are used to define the criteria of the Monte Carlo simulation for verification of the Autoland function in Section 6.

For the intended approach procedure, a Satellite Based Augmentation System (SBAS) shall be used. For SBAS, a Global Navigation Satellite System (GNSS) Landing System Sensor Unit (GLSSU) compatible with ARINC-743B provides the required signals for the flight along the glide path using SBAS signals for GNSS augmentation:

- Rectilinear horizontal (lateral) deviation Δy_{LOC} (ARINC 429, Label 116),
- Rectilinear vertical deviation ΔH_{GS} (ARINC 429, Label 117),
- Distance to threshold x_{THR} (ARINC 429, Label 177),

where rectilinear deviation denotes the perpendicular distance of the A/C's position from the desired glide path. It is assumed, that the A/C is able to land automatically, if a Ground Based Augmentation System (GBAS) is used instead to provide the required signals for guidance along the glide path. Additionally, the A/C incorporates a high precision radar altimeter that provides the height above ground for the final landing phase until touchdown. The height above ground signal is exclusively used when the A/C is over the runway that is assumed to be flat. The Autoland function is developed for runways that meet the aerodrome conditions that are defined for commercial transport A/C in [2], AMC AWO.A.ALS.106, Section 5.2. In particular, the required maximum landing distance of 823 m is quite large. Due to its low approach airspeed, the A/C can come to a full stop much earlier. Therefore, all flare function concepts that Lambregts [18] discusses, including the direct control of the vertical speed, are applicable irrespective of the individual influence on the landing distance.

The Autoland function shall achieve simultaneous contact of the two main wheels of the landing gear and the tail wheel at a target pitch angle $\Theta_{TD} \approx 2°$ (known as a three-point landing) to avoid excessive pitch movement after touchdown. If the pitch angle at touchdown is excessive, the tail wheel makes ground contact first, potentially exceeding the structural load limits. Conversely, if the pitch angle is too low, the main wheel touches the ground first at a high sink rate, causing the angle of attack to increase, and the A/C will become airborne again and will bounce on the runway - potentially with a too high sink rate. Therefore, in addition to precise tracking of the approach airspeed and vertical speed, the Autoland function has to ensure that the pitch attitude remains within specified tolerances at touchdown.

In comparison to commercial transport A/C, the taildragger A/C employs a higher approach airspeed V_{APP} of nearly double the stall speed V_S. This unusual high ratio V_{APP}/V_S (typically $V_{APP} = 1.3\,V_S$ plus additions for wind and turbulence) is required to provide a sufficient absolute margin to the low stall speed, accounting for turbulent conditions, gusts, and especially wind shear situations.

Additionally, a higher approach speed allows for enhanced manoeuvrability, particularly about the roll axis, as control surfaces exhibit greater effectiveness at higher dynamic pressures. To prevent prolonged floating over the runway, the Autoland function shall aim for distinct touchdown at a sink rate of $\dot{H}_{TD} = -0.5$ m/s. This descent rate ensures a controlled touchdown, minimizing the risk of a prolonged flight in the ground effect and aiding in maintaining stability and control.

DOI: 10.13009/EUCASS2023-949

Table 1 lists the required maximum operational values for headwind, tailwind and crosswind. For the specified maximal lateral wind component, the A/C heading does not need to be aligned with the runway centre line at touchdown. To avoid excessive lateral forces, the A/C incorporates a swivel-mounted main landing gear. Therefore, a de-crab before touchdown is not required.

Table 1: Operational maxima of stationary wind components

Wind component	Operational maximum
Headwind [m/s]	6
Tailwind [m/s]	2
Crosswind [m/s]	3

It is assumed, that the structural loads of the main landing gear during touchdown are within the defined limits, if the specified values for maximum sink rate, airspeed and maximum crab angle at touchdown stay within their specified limits. However, the maximum forces at the landing gear are an additional requirement as listed in Table 2. Because of the unusual high glide ratio of the A/C, the landing gear and the speed brakes have to be fully extended to acquire and stabilize a -3° glideslope with some margin for corrections of deviations that are caused e.g. by atmospheric disturbances. Therefore, the speed brakes cannot be used as a means to control the total energy of the A/C by increasing the drag while the Autoland function is active.

Table 2: Performance requirements for the Autoland function

Requirement	**Limit**		**Risk Limit**	**Reference**
	Min	Max		
Height above ground 60 m behind the runway threshold $h_{xTHRS,60m}$ [m]	0	-	Average risk: 10^{-6} 1/landing Limit risk: 10^{-5} 1/landing	[2] AMC AWO.A.ALS.106, 1.4 a) b)
Distance between the threshold and the touch down point x_{TD} [m]	-	823/ 914		[2] AMC AWO.A.ALS.106, 1.4 a) b)
Sink rate at the touchdown $\dot{h}_{TD}$ [m/s]	-1.3	-		[2] AMC AWO.A.ALS.106, 1.4.1 a)
Structural load on main landing after touchdown in z-direction of the A/C-fixed coordinate system F_z [N]	-	26531		[2] AMC AWO.A.ALS.106, 1.4 d)
Airspeed precision along the glidepath segment below 400 ft above ground and ahead of the threshold $2\sigma\delta V_{CAS,GP}$ [m/s]	-2.57	2.57	2σ	[3] ED-283 3.5.7.4
Between 300 ft and 100 ft above the runway, the vertical deviation from the glide path shall never exceed the deviation alert limit.	altitude dependent		-	adaption of [3] ED-283 3.5.7.3

4. Automatic Landing Procedure

The Autoland procedure is developed to comply with the applicable ICAO standards and recommended practices [4] while simultaneously considering the specific characteristics of the “StratoStreamer” A/C. The landing trajectory is fully defined by a list of three consecutive waypoints in a flight plan. SBAS provides the geometry of the -3° glide path. It is assumed, that the received flight plan is always well-defined and that the A/C performance allows to follow the trajectory with sufficient margin at V_{APP}. In a flight plan, the three consecutive waypoints

- Intermediate Fix (IF),
- Landing Threshold Point (LTP) and
- Departure End of Runway (DER)

define a landing sequence. The runway itself is fully defined by the two waypoints LTP and DER assumed to be the runway centre line.

Figure 4 illustrates the vertical and lateral profile of an automatic landing procedure, which is a sequence of six consecutive phases. During Autoland, the FCL SW will consecutively pass through all phases. A transition from one phase to the next phase is triggered, when all entry criteria of the next phase are met. Additionally, a go-around may be initiated by the FCL SW in case of discontinued sensor signals. Furthermore, a landing can be terminated by an external demand from a remote pilot at a ground station. Phases are denoted by Roman numerals, transitions are

DOI: 10.13009/EUCASS2023-949

denoted by encircled Arabic numerals. The number of a transition denotes the consecutive number of the phase that is entered.

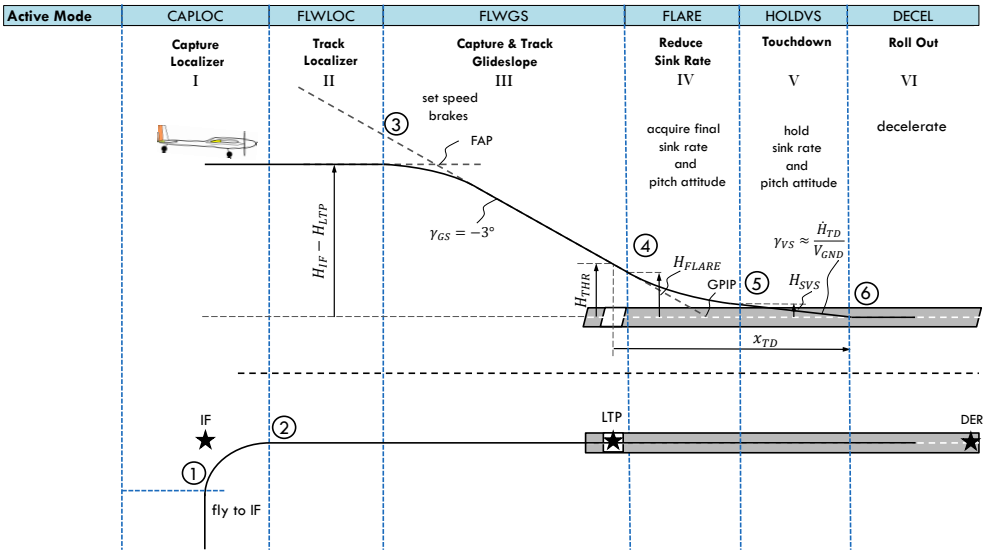

Figure 4: Vertical and lateral profile of the Autoland sequence

Prior to activation of the Autoland function, the A/C flies towards the Intermediate Fix (IF) at or around the intermediate approach altitude H_{IF} above MSL. It is assumed, that the IF is reached at the intermediate approach altitude. If the intermediate approach altitude is not acquired until the IF is reached, the FCL tries to acquire the altitude in the first two phases of the Autoland sequence (similar to the intermediate approach segment) until the Final Approach Point (FAP) is reached and the final approach segment is entered. However, the FCL can only follow the landing procedure if the altitude deviation at the IF is not excessive, as the A/C performance limits its maximum sink rate. In more detail, the automatic landing consists of the consecutive phases:

I. **Capture Localizer (CAPLOC):** If all entry conditions for an Autoland sequence are met, the A/C turns into the direction of the runway (transition ①). The FCL uses the intermediate approach altitude H_{IF} as altitude command. For the full Autoland sequence until touchdown, the FCL memorizes the commanded airspeed V_{APP} of this phase as commanded approach airspeed. V_{APP} can be adapted by the remote pilot to the actual wind conditions before the approach has to be stabilized in phase III.

II. **Track Localizer (FLWLOC):** If the localizer track to the LTP is acquired (transition ②), the FCL have to control the rectilinear lateral deviation from the glide path (localizer deviation that the GLSSU determines). The FCL track the localizer until the end of the Autoland sequence. The FCL hold the intermediate approach altitude H_{IF} and the approach airspeed V_{APP}.

III. **Capture and Track Glideslope (FLWGS):** When transition ③ is reached, the FCL intercept the -3° glideslope at the Final Approach Point (FAP) from below and initiates the final approach segment. Simultaneously, the speed brakes and flaps are set to the approach configuration to enable the required sink rate. Based on the trim results for different approach configurations, a positive (downward) flap deflection is required to increase the drag. Consecutively, the FCL have to control the rectilinear vertical deviation from the glide path (glideslope). The glideslope crosses the LTP at a height above ground H_{THR} and intersects the runway at the Glidepath Intercept Point (GPIP). The A/C tracks the localizer and holds the approach airspeed V_{APP}.

IV. **Reduce Sink Rate (FLARE):** At a defined height above ground H_{FLARE} behind the LTP (transition ④), the sink rate is reduced to a rate $\dot{H}_{TD}$ that is suitable for the touchdown. The sink rate that is used as reference by the FCL in this phase is referenced to the ground. The FCL track the localizer and holds the approach airspeed V_{APP}. The flaps are pre-set to a landing configuration depending on the approach airspeed V_{APP}.

V. **Touchdown (HOLDVS):** When the sink rate for the touchdown $\dot{H}_{TD}$ is acquired (transition ⑤), Autoland switches the FCL have to ensure that the sink rate is within the boundaries for a safe landing. It is assumed, that $\dot{H}_{TD}$ is stabilized until the A/C passes the altitude above ground H_{SVS} that is used as activation criterion for HOLDVS. In this phase, the FCL have to hold a defined pitch attitude Θ_{TD} that is required for a three-point landing until touchdown. The FCL track the localizer and holds the approach airspeed V_{APP}. At a low altitude above the runway, the thrust can be reduced to idle to reduce the airspeed (kinetic energy) at touchdown.

VI. **Roll Out (DECEL):** If the weight-on-wheel sensors indicate that the A/C touched the ground (transition ⑥), the Autoland switches into the FCL mode that controls the A/C on ground. The thrust is reduced to idle. After touchdown, speed brakes and flaps are fully negatively extended to immediately increase drag and reduce lift. The

DOI: 10.13009/EUCASS2023-949

FCL track the localizer, decelerate to the taxi-speed V_{RWY} or command to a full stop while the FCL hold a bank attitude of $\Phi = 0$ °.

5. Total Energy Based Controller Structure and Controller Synthesis

A cascaded controller structure is selected to control the longitudinal A/C motion. Lambregts's control concept of the Total Energy Control System (TECS) [5], [6], [7] is applied to decouple the speed and the flight path angle dynamics. Considering the A/C a rigid body, the total energy E is the sum of its kinetic energy E_{kin} and its potential energy E_{pot}:

$$E = E_{kin} + E_{pot} \quad \text{, with} \tag{1}$$

$$E_{kin} = \frac{1}{2} \cdot m \cdot V_K^2 \quad , \tag{2}$$

$$\dot{E}_{kin} = m \cdot V_K \cdot \dot{V}_K \quad , \tag{3}$$

$$E_{pot} = m \cdot g \cdot H \quad \text{, and} \tag{4}$$

$$\dot{E}_{pot} = m \cdot g \cdot \dot{H} \quad . \tag{5}$$

In order to alter the total energy of the system, it is necessary to either perform work W on the system or dissipate energy from it. The derivative of work with respect to time is defined as power P. Therefore, the power is equivalent to the change of the total energy $\dot{E}$:

$$P = \dot{E} = \dot{E}_{kin} + \dot{E}_{pot} \quad . \tag{6}$$

Substituting equation (3) and (5) into equation (6) and dividing by the A/C weight $m \cdot g$ yields the specific excess power:

$$\frac{\dot{E}}{m \cdot g} = V_K \frac{\dot{V}_K}{g} + \dot{H} \quad . \tag{7}$$

The first control variable of TECS is a dimensionless formulation of the specific excess power (or energy angle [9]) that equals equation **(7)** divided by the speed V_K:

$$\dot{E}_s = \frac{\dot{V}_K}{g} + \frac{\dot{H}}{V_K} = \frac{\dot{V}_K}{g} + \sin\gamma \quad . \tag{8}$$

Consequently, the relative engine power demand P_c is selected as actuating variable. The power demand P_c is equally distributed to both engine power demands $P_{L,c}$ and $P_{R,c}$. The second control variable of the TECS is the specific energy distribution rate $\dot{L}$ that describes the distribution of the specific excess power between kinetic energy and potential energy:

$$\dot{L} = -\frac{\dot{V}_K}{g} + \frac{\dot{H}}{V_K} \quad . \tag{9}$$

As proposed in [7], the specific excess power is distributed through the pitch angle demand Θ_c as actuating variable by a pitch angle controller that utilizes the elevator η for pitch control. Therefore, TECS particularly suits the energy-optimal A/C operation, because the engines are exclusively used to change the total energy of the system. The control of the specific energy distribution rate $\dot{L}$ directly compensates the altitude error if the A/C flies below the commanded altitude by exchanging energy from excessive airspeed. Vice versa, excessive altitude can be given up to compensate for the airspeed error when falling below the commanded speed without changing the engine power demand.

The classical TECS controls both control variables $\dot{E}_s$ and $\dot{L}$ by proportional-integral control [5]. The recommendation in [10] and [11] to only use an integral controller to control $\dot{E}_s$ is suitable for the "StratoStreamer" A/C, because the fast response of the electrical engines already ensure sufficient bandwidth. It is assumed, that the engines are controlled by the shaft power as control variable. The change of the power demand ΔP_c is calculated from required change of propulsive power ΔP_{Prop} by considering the engine efficiency η_{Eng} and the propulsion efficiency η_{Prop}:

DOI: 10.13009/EUCASS2023-949

$$\Delta P_c = \eta_{Eng} \cdot \eta_{Prop} \cdot \Delta P_{Prop} = \eta_{Eng} \cdot \eta_{Prop} \cdot \Delta F_c \cdot V_A \quad . \tag{10}$$

The required thrust change ΔF_c is calculated from the error of the specific excess power $\Delta \dot{E}_s$ by

$$\Delta F_c = m \cdot g \cdot \Delta \dot{E}_s \cdot G_{i,E} \cdot \frac{1}{s} \quad . \tag{11}$$

Depending on the requirement, the total energy can be referenced to the surrounding air mass instead of the earth as inertial system or to a blend of both values to improve the controller performance in wind shear conditions [11]. For the automatic landing, total energy is referenced to air speed. Due to the noise of the airspeed measurement, the feedback of the measured airspeed V_A and its derivative $\dot{V}_A$ are realized by feeding back estimated signals from a complementary filter $\hat{V}_A$ and $\hat{\dot{V}}_A$. The controlled states $\dot{E}_s$ and $\dot{L}$ are calculated in the TECS from the commanded acceleration $\dot{V}_{A,c}$ and for small angles from commanded flight path angle:

$$\gamma_c \approx \sin \gamma_c = \frac{\dot{H}_c}{\hat{V}_A} \quad . \tag{12}$$

Figure 5 shows the resulting cascaded controller structure. The pitch control function forms the innermost cascade that is utilized by the TECS. Since both control variables of the TECS are operated on actuating variables that are limited in value and rate, Anti-Windup provisions are incorporated into both control paths of the TECS that intermit the integration if either the pitch command Θ_c or the engine power demand P_c saturates. This measure allows to adapt TECS in particular to a varying maximum engine power that highly depends e.g. on the charging status of batteries.

If either of the actuating variables saturates, the speed priority of the TECS activates and differing from equation **(9)**, the control error of the specific energy distribution rate $\dot{L}$ is calculated by:

$$\Delta \dot{L} = -\frac{\Delta \dot{V}_A}{g} \quad . \tag{13}$$

Thereby, the energy is distributed with full priority to the kinetic energy which ensures that the acceleration and consequently the airspeed can be controlled without changing the transfer behaviour. The flight path angle is set due to the remaining specific excess power of the total energy control path which can also result in a pitch down response to trade off altitude for airspeed.

Based on the TECS, the outer cascade is formed by two independent control functions to control airspeed and altitude of the A/C. The airspeed control function is referenced to the equivalent airspeed V_{EAS} and calculates the acceleration $\dot{V}_{A,c}$. The altitude control function calculates the commanded flight path angle command γ_c. The commanded altitude H_c can be either referenced to barometric altitude H_{BAR}, the altitude over mean sea level H_{MSL} or the altitude above ground H_{GND} depending on the operational requirements. Within the cascaded controller structure, the bandwidth of the control functions has to decrease from the inner to the outer cascades. Cascades should be separated in bandwidth by at least by a factor two, better by a factor of 4 to prevent reduced damping [10].

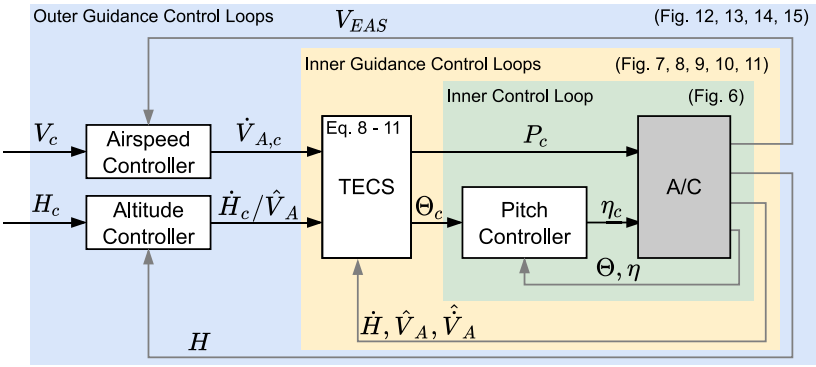

Figure 5: Cascaded controller structure for the longitudinal motion

The innermost control loop that provides pitch control is optimized to unify the pitch dynamics throughout the flight envelope. The design and optimization of the pitch controller is a standard task and not subject of this paper. The synthesis considers a generalized system delay of 100 ms in each feedback loop. The pitch controller is tuned by MOPS [16] to meet the design criteria that are listed in Table 3. Figure 6 shows the Bode diagram for the transfer function $F_{\Theta\Theta_c}$ from Θ_c to Θ throughout the full airspeed range at 3300 ft.

DOI: 10.13009/EUCASS2023-949

Table 3: Tuning criteria for the Θ control loop

Criterion	Acceptable Values
Bandwidth [rad/s]	$\omega_\Theta > 1.2$
Damping [-]	$D > 0.7$
Real part of all poles [1/s]	$Re < 0$
Gain margin [dB]	$GM > 6$
Phase margin [°]	$PM > 45$

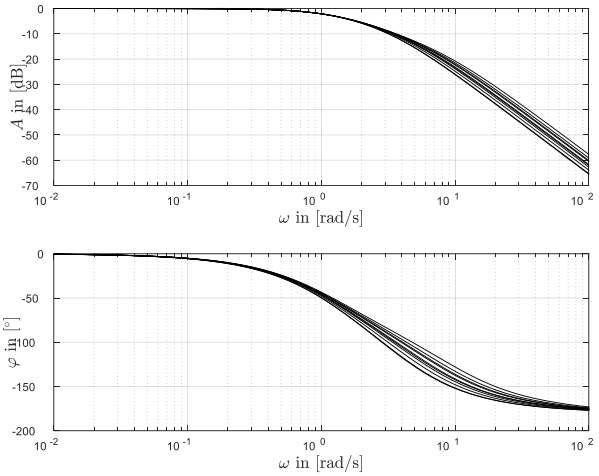

Figure 6: Bode diagram for $F_{\Theta\Theta_c}$ at 3300 ft

Because the pitch control function sufficiently unifies the A/C pitch dynamics, the design of TECS and the superordinate altitude and airspeed control functions require only a single set of gains for all trim points. Table 4 lists the design criteria for the TECS, Table 5 the criteria for the altitude and airspeed controller. The Bode diagram for the transfer function $F_{\dot{V}\dot{V}_c}$ from $\dot{V}_{A,c}$ to $\dot{V}_A$ through the full airspeed range at flight level FL033 is depicted in Figure 7, for the transfer function $F_{\gamma\gamma_c}$ from γ_c to the γ in Figure 8. The transfer functions $F_{\dot{V}\gamma_c}$ and $F_{\gamma\dot{V}_c}$ that characterize the coupling of the airspeed and flight path dynamics are plotted as dotted lines. The dynamics are sufficiently decoupled, as the amplitude separation of $F_{\dot{V}\gamma_c}$ and $F_{\gamma\dot{V}_c}$ from $F_{\dot{V}\dot{V}_c}$ and $F_{\gamma\gamma_c}$ is greater than 30 dB (γ in rad, $\dot{V}$ in m/s²) for all frequencies up to the design bandwidth. Figure 9 visualizes the decoupled dynamics. A step input to $\dot{V}_{A,c}$ results in small flight path angles and vice versa, a step input in γ_c induces only small accelerations $\dot{V}_A$. The TECS does not need to provide guidance accuracy for the transfer function $F_{\dot{V}\dot{V}_c}$, because the superordinate airspeed control loop is accurate by feeding back $V = \int \dot{V}$. The Nichols charts for both loops of the TECS in Figure 10 and Figure 11 indicate sufficient gain and phase margins through the full airspeed range at 3300 ft.

Table 4: Tuning criteria for the TECS control loops

Criterion	Acceptable Values
Bandwidth [rad/s]	$0.5 > \omega_{TECS} > 0.4$
Damping [-]	$D > 0.5$
Real part of all poles [1/s]	$Re < 0$
Gain margin [dB]	$GM > 6$
Phase margin [°]	$PM > 45$

Table 5: Tuning criteria for V_{EAS} and H control loops

Criterion	Acceptable Values
Bandwidth [rad/s]	$\omega_H, \omega_V < 0.1$
Damping [-]	$D > 0.5$
Real part of all poles [1/s]	$Re < 0$
Gain margin [dB]	$GM > 6$
Phase margin [°]	$PM > 45$
Overshoot [m/s]/[m]	$OS = 0$

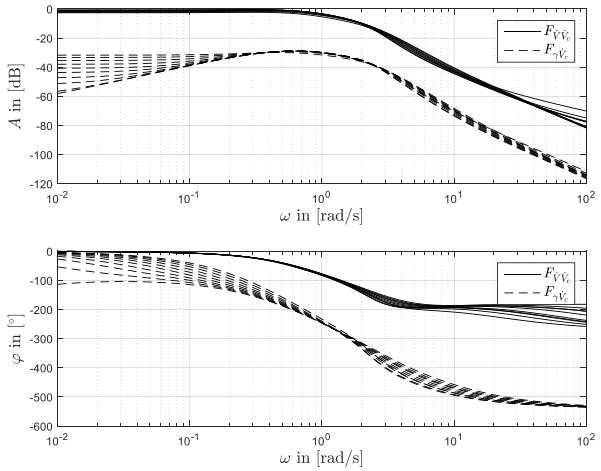

Figure 7: Bode diagram for $F_{\dot{V}\dot{V}_c}$ and $F_{\gamma\dot{V}_c}$

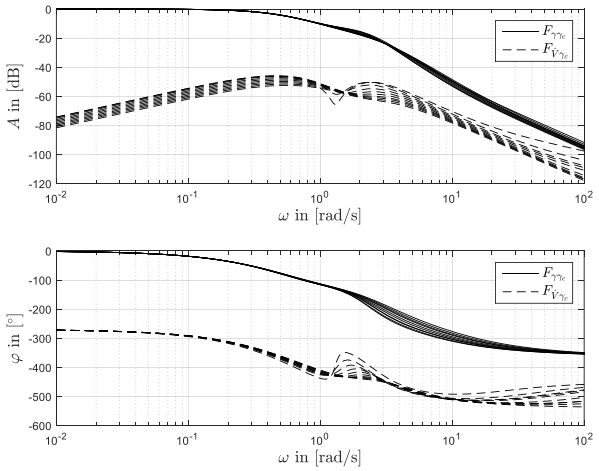

Figure 8: Bode diagram for $F_{\gamma\gamma_c}$ and $F_{\dot{V}\gamma_c}$

DOI: 10.13009/EUCASS2023-949

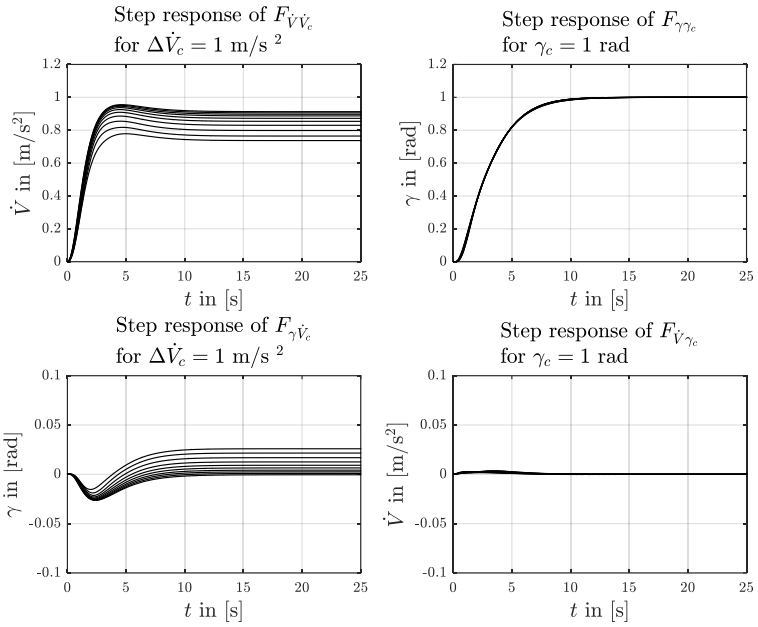

Figure 9: TECS step input responses of the TECS control loops

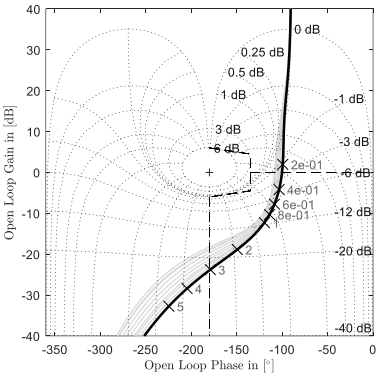

Figure 10: Step input response of $F_{\gamma\gamma_c}$

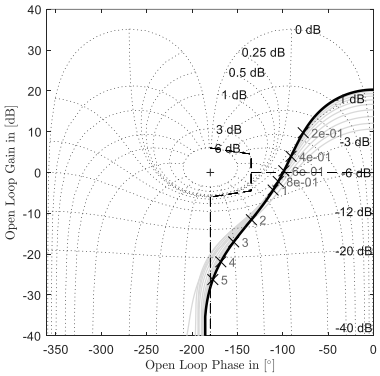

Figure 11: Nichols chart $F_{\dot{V}\dot{V}_c}$

As TECS sufficiently decouples airspeed and altitude dynamics, the altitude and the airspeed control functions can be individually designed as proportional controller with a single gain set. Figure 12 shows the step response of the altitude controller through the full airspeed range at flight level FL033, Figure 14 the resulting Bode diagram for the transfer function F_{HH_c} from H_c to the H. Equivalently, Figure 13 shows the step response of the airspeed controller, Figure 15 the resulting Bode diagram for the transfer function F_{VV_c} from V_c to V_{EAS}.

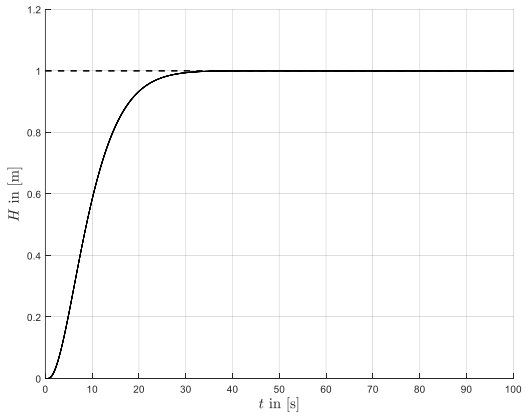

Figure 12: Step input response of F_{HH_c}

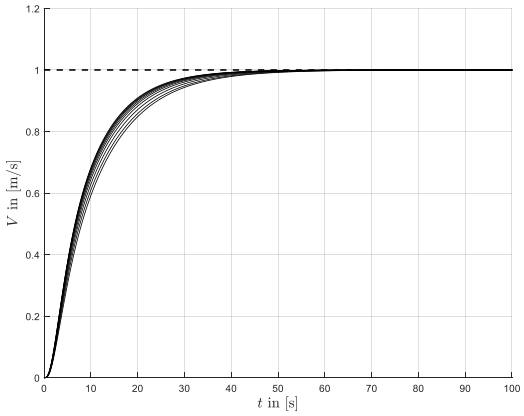

Figure 13: Step input response of F_{VV_c}

DOI: 10.13009/EUCASS2023-949

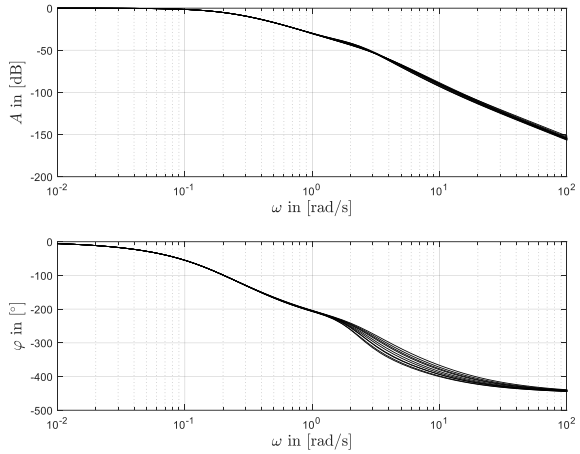

Figure 14: Bode diagram for F_{HH_c}

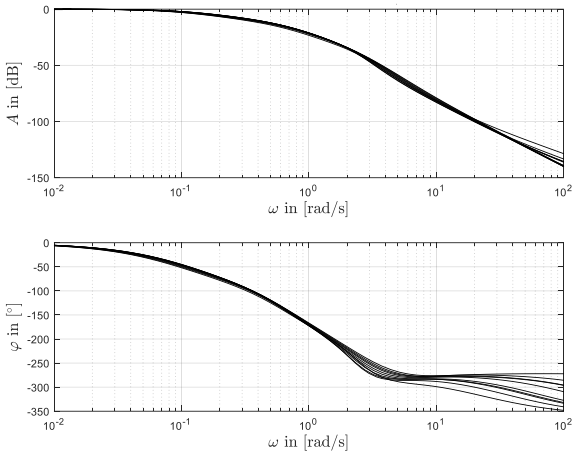

Figure 15: Bode diagram for F_{VV_c}

The described control functions are used for Autoland phases I and II until the A/C intercepts the glideslope. Upon activation of phase III (FLWGS), the control error in the altitude controller is replaced by the rectilinear vertical deviation from the glide path ΔH_{GS}. Additionally, the sink rate $\dot{H}_{GS}$ that equals the glideslope γ_{GS} at the current ground speed V_{GND} is introduced as feed forward command that ensures guidance accuracy. The adaptions of the altitude controller are marked green in Figure 16. Simultaneously, the speed brakes and flaps are set to pre-defined deflections to increase the drag to enable the -3° approach. Therefore, the speed brakes are fully deflected. The flaps are set to a positive deflection $\eta_{F,GS}$ to increase the wing's camber. At a constant V_{APP}, TECS consequently commands a lower Θ and the angle of attack α decreases below the aerodynamic optimum, which results in increasing drag.

For this purpose, a flap control function is incorporated in parallel to the pitch controller in the cascaded controller structure (see Figure 17). When the A/C crosses the runway threshold and passes through a defined height above the runway, phase IV (FLARE) activates. In this phase, the sink rate is reduced to a value that is suitable for touchdown. TECS receives this touchdown sink rate $\dot{H}_{TD}$ as target value. Additionally, the ground-referenced sink rate $\dot{H}_{GND}$ is fed back to TECS to enable control of sink rate referenced to the runway. The flaps are set to the pre-defined deflection $\eta_{F,TD}$ that suits an ideal three-point landing at the given approach airspeed V_{APP} with the intended sink rate for touchdown $\dot{H}_{TD}$.

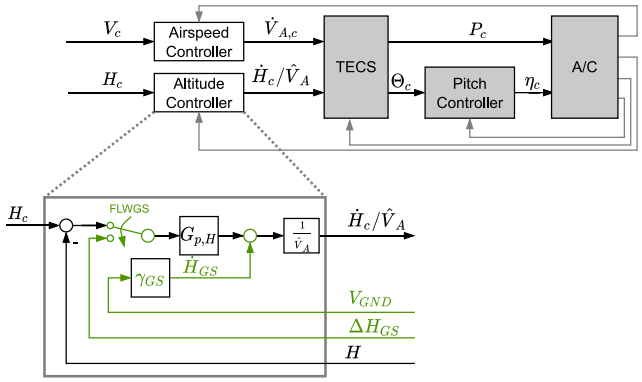

Figure 16: Controller adaptions for landing phase III

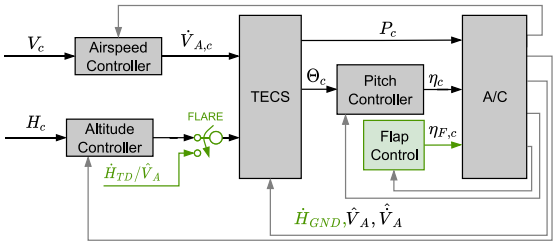

Figure 17: Controller adaptions for landing phase IV

After the A/C is stabilized around $\dot{H}_{TD}$ and when the A/C passes H_{SVS} above the runway, phase V (HOLDVS) activates. In this phase, the FCL shall ensure that the touchdown occurs within tight limits with the intended pitch attitude Θ_{TD}, the approach airspeed V_{APP} and the target sink rate $\dot{H}_{TD}$. Landings with the controller structure that controls $\dot{H}$ and V through TECS may lead to excessive pitch attitudes at touchdown arising from the distribution of the specific excess power between kinetic energy and potential energy by the TECS [10]. Additionally, pitch attitude, vertical speed and airspeed are not independently controllable by the actuating variables elevator η and engine power demand P_c. As the flap function has a direct influence on the lift, in particular because of the impact of the inner flaperon pair, a proportional controller is integrated into the flap control function that directly controls the vertical speed $\dot{H}$ in a Direct Lift Control (DLC) like manner.

To integrate this function into the existing controller structure, the changes that are marked green in Figure 18 are required. Notably, the decoupling of airspeed and altitude dynamics is suppressed by neglecting the share of the acceleration error $-\Delta\dot{V}_A/g$ in the calculation of the control error of the specific energy distribution rate $\Delta\dot{L}$ (marked orange in Figure 18). This TECS mode of operation is known as path-priority, as it distributes all specific excess power

DOI: 10.13009/EUCASS2023-949

to influence the required vertical speed. Hence, the specific energy distribution rate $\dot{L}$ and consequently the pitch angle command of TECS Θ_{TECS} are only influenced by the difference of current sink rate and intended sink rate at touchdown. The intended pitch attitude Θ_{TD} is used as command variable of the pitch control loop ensuring a three-point landing. Each deviation of Θ_{TECS} from Θ_{TD} is reinterpreted as sink rate error and subsequently as command variable $\Delta\Theta_{VS}$ for the flap control function. The total energy control path is preserved and ensures low-bandwidth airspeed control.

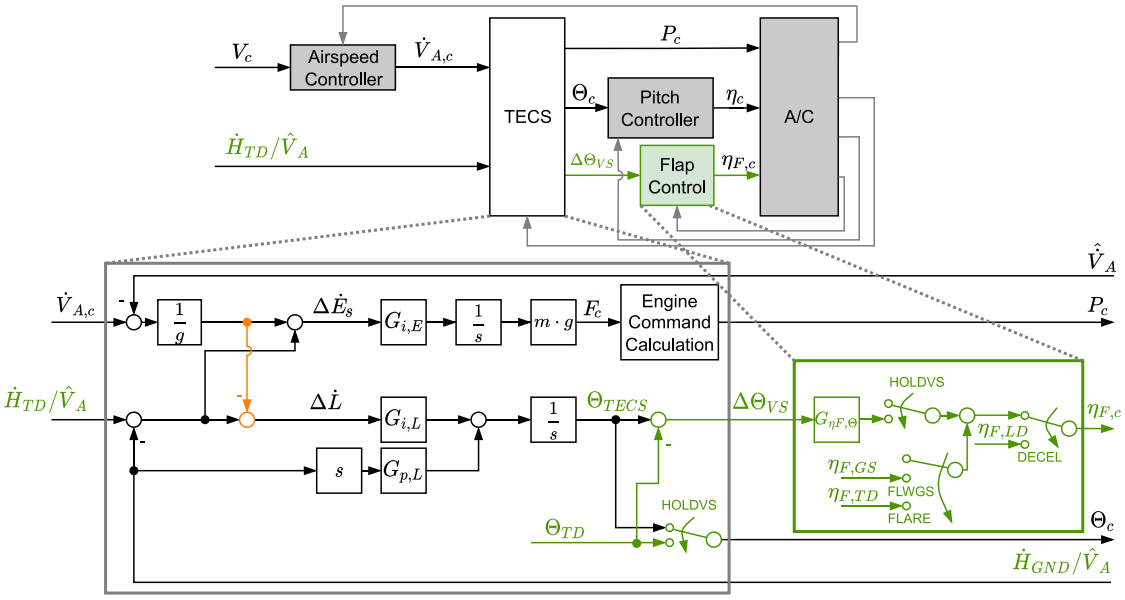

Figure 18: Controller adaptions for landing phase V

The proportional gain $G_{\eta F,\Theta}$ of the flap control function is tuned to preserve transfer behaviour of the vertical speed path that is depicted in Figure 9. This requirement ensures that bandwidth separation of the airspeed control function, the vertical speed control through the flaps and the pitch control function are preserved. Adding the flap control function enables separate control of Θ, $\dot{H}$ and V for landing phase V. The step responses of the three control variables to the respective inputs in the three control functions that is depicted in Figure 19 validate the intended decoupling of Θ, $\dot{H}$ and V for the final landing segment until touchdown.

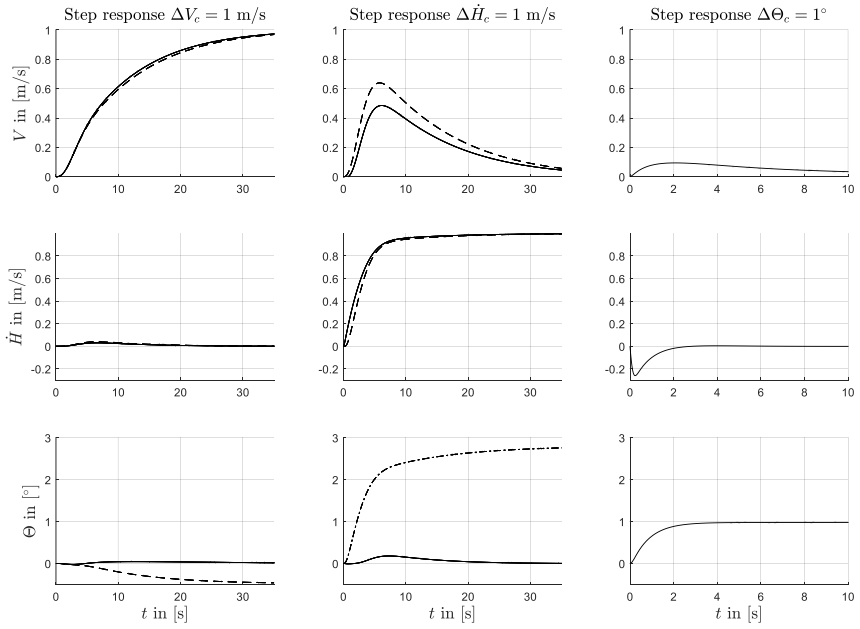

Figure 19: Responses to step inputs in V_c , γ_c and Θ_c, solid line: adapted TECS with flap control function, dashed line: conventional TECS in path priority

The algorithms of the FCF are implemented as FCL in Simulink/Stateflow and integrated into the non-linear flight simulation of the HAPS. Figure 20 shows time histories of a nominal landing without wind or turbulence in the non-

DOI: 10.13009/EUCASS2023-949

linear simulation environment. The simulation starts at an altitude of 500 ft above ground with the A/C aligned with the runway and landing gear extended. After around 5 s, the Autoland function activates and directly passes through phase I and II, as the A/C is already aligned with the runway and the glideslope can be intercepted from below. The flaps are set to around $\eta_F = 3°$ while the A/C acquires the glideslope angle $\gamma_{GS} = -3°$. After the glide slope is acquired, the rectilinear vertical deviation from the glideslope ΔH_{GS} and the deviation from the approach airspeed ΔV_{EAS} are zero until the A/C reaches the threshold at $H_{GND} = 50$ ft above the runway after around 135 s. When phase IV activates, TECS acquires the target sink rate $\dot{H}_{TD} = -0.5$ m/s by increasing the thrust and pitch attitude. The activation of the path priority is visible as the airspeed initially deviates from V_{APP} by around 1 m/s after the transition from phase III to phase IV. Additionally, the flaps η_F are negatively extended to the touchdown configuration which further increases the pitch up motion to the target pitch angle of $\Theta_{TD} \approx 2°$. After transition from phase IV to phase V, the flaps are used to control the vertical speed. The reallocation of the actuating variables does not result in any transient behaviour. The target values $\dot{H}_{TD}$ and Θ_{TD} are perfectly held until touchdown (transition from phase V to phase VI) while the airspeed controller slowly reacquires V_{APP}. After touchdown, the flaps are set to the lift-dump position $\eta_F = -10°$ and the A/C starts to decelerate.

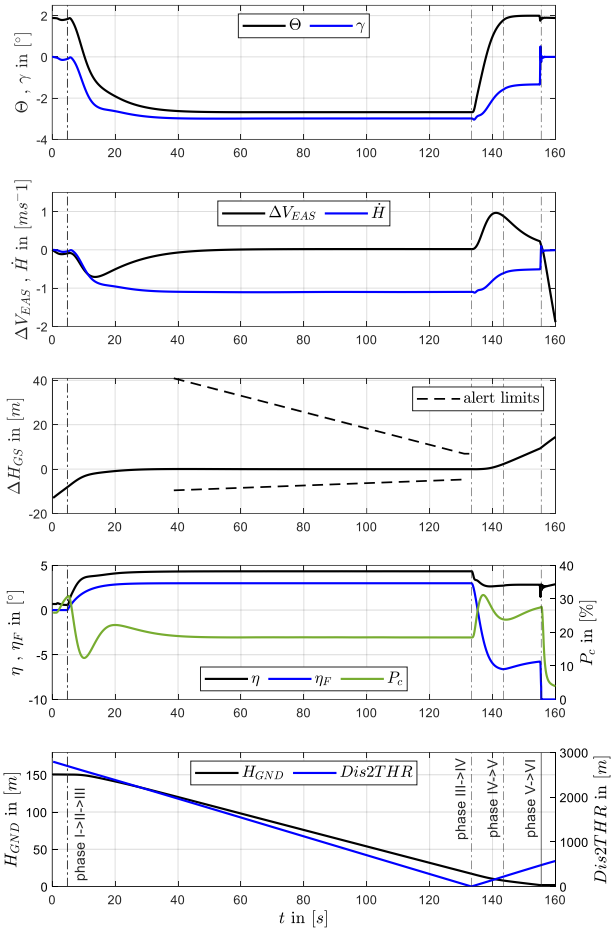

Figure 20: Vertical profile of a nominal landing

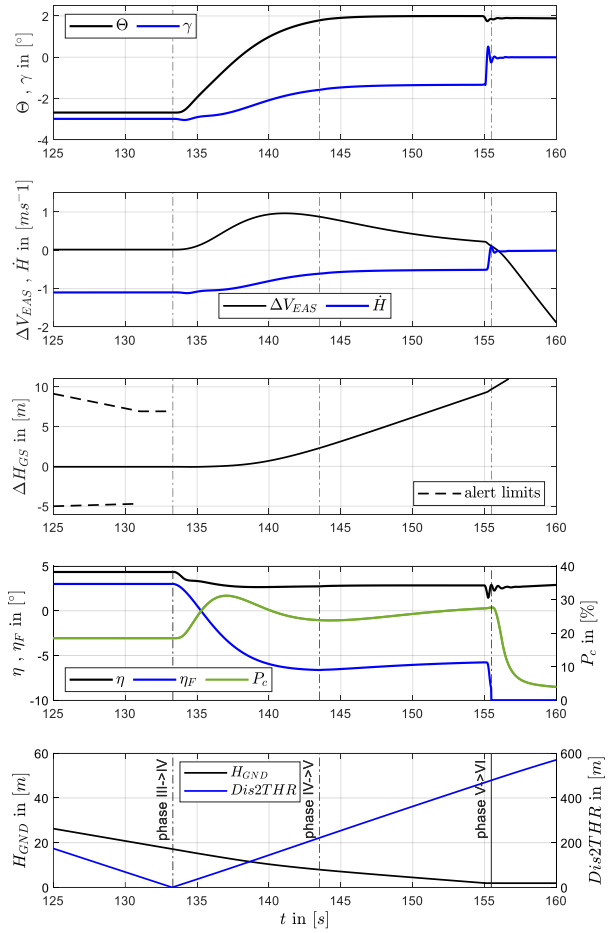

Figure 21: Vertical profile of landing phase IV and V

6. Verification

To verify the robustness of the FCL design against the requirements for the Autoland function described in Section 3, a Monte Carlo simulation is conducted in a similar manner as required by EASA for commercial transport A/C [2]. The Monte Carlo simulation is a stochastic procedure that utilizes a large number of random experiments (here 5000 approaches) to establish hidden correlations through probability theory. In the context of demonstrating the robustness of the Autoland function, Monte Carlo simulations involve varying A/C parameters and environmental conditions randomly. Distribution functions, such as uniform or Gaussian normal distribution, are assigned to these parameters. The average risk in a Monte Carlo simulation is evaluated by randomly varying all influencing parameters. On the

DOI: 10.13009/EUCASS2023-949

other hand, the limit risk is determined by fixing one parameter at its extreme value while randomly varying all other parameters according to their respective probability distributions.
For all approach simulations, criterion values are determined and compared against predefined limits. Afterwards, the distribution of criterion values across all simulations is approximated using both the normal distribution and an automatically determined best-fit distribution. Based on the approximated continuous distribution functions, the probability of exceeding the criterion limits is directly calculated from the probability distribution function. The approximation and risk determination are automatically carried out by the multi-objective design tool MOPS [16].

The individual simulations start at an altitude of 500 ft above ground with the A/C aligned with the runway, with extended landing gear and a fixed mass configuration. The mass of the A/C remains constant. The applied criteria are outlined in Table 2. In accordance with [2], the analysis focuses on assessing the average risk by varying the parameters specified in Table 6, while determining the probability of exceeding the defined limits. Furthermore, a limit risk analysis is performed to determine the probability of exceeding the limits with one parameter set to its extreme value. The wind conditions are defined at 10 m above ground. The wind and turbulence model used for simulations is based on wind model 1 in [2], where the turbulence characteristics depend on current airspeed, altitude above ground and the reference wind speed. A total of 5000 flight simulations are conducted to assess the average risk. 2000 flight simulations are performed each with maximum tailwind, headwind, and crosswind conditions.

Table 6: Parameter Variation for Average Risk Monte Carlo simulation

Parameter	**Notation**	**Limits**	**Unit**	**Distribution**	**Median**	**Std. Dev.**	**Reference**
Centre of Gravity	x_{cg}	[-6.875, -6.613]	m	uniform	-	-	-
Tail Wind/Head Wind	u_{10}	[-2, 6]	m/s	normal	0.77	3.91	[2]
Crosswind	v_{10}	[-3, 3]	m/s	normal	0	3.6	[2]
Runway Elevation	h_{RWY}	[-1000, 9200]	ft	uniform	-	-	-
Runway Slope	γ_{RWY}	[-0.458, 0.458]	°	normal	0	0.172	[2]
Temperature	T	[-45, 38]	°C	uniform	-	-	-

Figure 22 shows the probability density function f and the probability distribution F for the criterion $h_{xTHRS,60m}$, Figure 23 for the criterion x_{TD}. In all simulations, the A/C remains airborne 60 meters behind the runway threshold, eventually touching down at the latest 576 meters behind the runway threshold. If the Gaussian normal distribution (green-dotted line) is used to approximate the criterion values, the average risk for both criteria is significantly lower than 10^{-6} per landing. As anticipated, the A/C has the potential to come to a stop much earlier than required. If no ILS-alike glide path has to be followed, the overall landing distance can be effectively decreased, if the selected height above ground at the runway threshold is reduced below 50 ft. Then the A/C can initiate the landing flare closer to the touchdown zone. The airspeed controller demonstrates high precision during the glide path segment (see Figure 26), successfully maintaining V_{APP} with a worst-case two standard deviation of $2\sigma = -1.22$ m/s throughout all simulations. Across all simulations, there were no instances where a landing had to be aborted due to the vertical deviation from the glideslope exceeding the defined alert limits (see Figure 20). Between 300 ft and 100 ft above the runway, the altitude controller demonstrates high precision with two standard deviations 2σ between 5 % and 20 % of the alert limits (see Figure 27). It is noteworthy that the FCL tend to fly slightly above the -3° glideslope. This behaviour is attributed to the saturation of the thrust in its idle setting, limiting the FCL's ability to directly compensate for positive vertical deviations by reducing the total energy while simultaneously maintaining the airspeed.
However, the vertical speed at touchdown exceeds the acceptable limits in multiple simulations (see Figure 24). Using the most conservative approximation of the distribution function, the probability of exceeding the limit of $\dot{H}_{TD} = -1.3$ m/s is found to be unacceptably high, as the limit is exceeded in approximately 1 out of every 100 landings. The criterion for maximum sink rate at touchdown $\dot{h}_{TD}$ and the maximum load on the main landing gear F_z (see Figure 25) correlate - as it is expected. The limit risk analysis revealed similar issues with the sink rate, in particular, where the steady headwind component is held at its maximum of 6 m/s. Detailed analyses of the time histories of the worst-case results indicate difficulties to compensate the simulated vertical turbulence due to the A/C's low wing loading and the resulting very low approach speed. The amplitude of the turbulence depends on the reference airspeed at a height of 10 m. Therefore, the worst cases occur when both steady headwind and crosswind values are close to their maxima. In particular, the turbulence model according to [2], which is defined for commercial transport A/C, generates gusts of a constant high amplitude with increasing frequency when the A/C approaches the ground. The vertical gust amplitudes right above the runway already exceed the supposed maximum vertical speed for the touchdown. Additionally, the frequency is so excessive, that the vertical speed controller is not able to follow the alternating up- and downwind gusts. If the gust direction changes from up to downwind right before touchdown, the A/C descends with the air mass and the criterion $\dot{h}_{TD}$ is immediately violated. It needs to be validated whether the relatively large vertical turbulence that the turbulence model generates close to ground is realistic. Whereas the CS-AWO turbulence model [2] seems to

DOI: 10.13009/EUCASS2023-949

be adequate for CS-25 transport category, it needs to be investigated if it is suited for A/C with low wing loading and a very low approach speed at ground heights below 10 m.

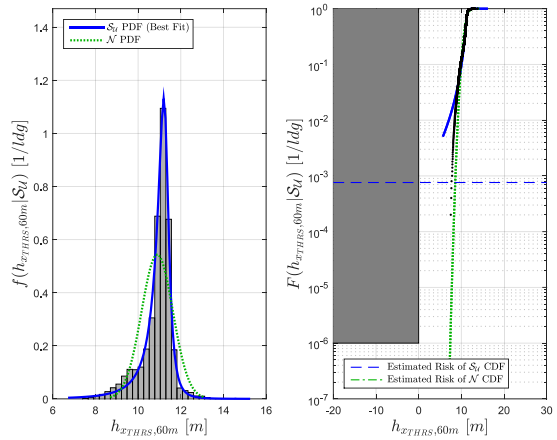

Figure 22: Distribution and estimated risk- $h_{xTHRS,60m}$

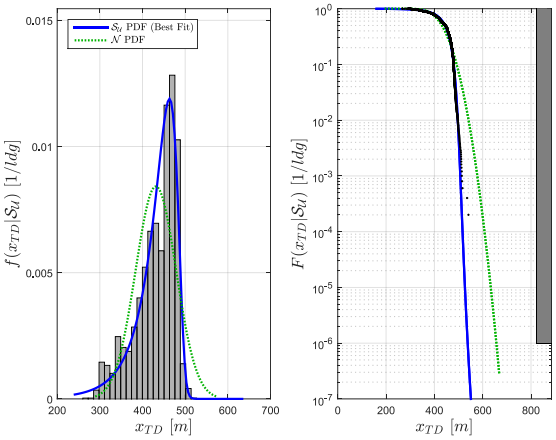

Figure 23: Distribution and estimated risk- x_{TD}

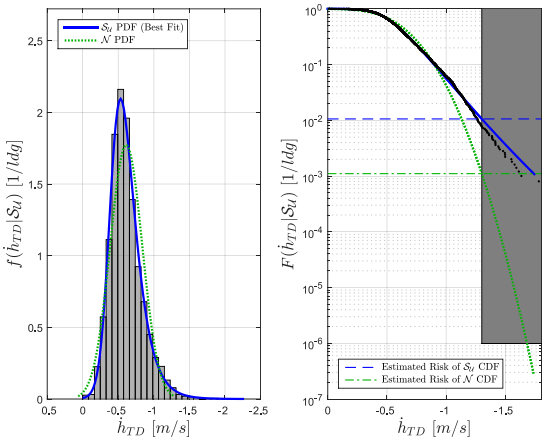

Figure 24: Distribution and estimated risk- $\dot{h}_{TD}$

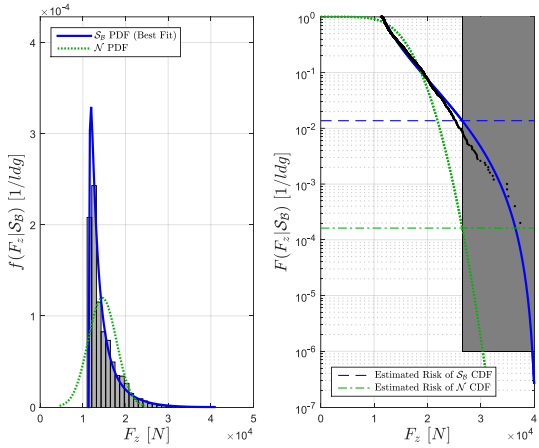

Figure 25: Distribution and estimated risk- F_z

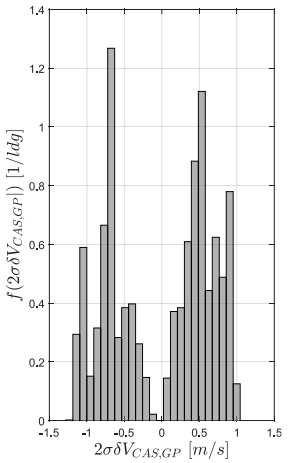

Figure 26: Distribution- $2\sigma\delta V_{CAS,GP}$

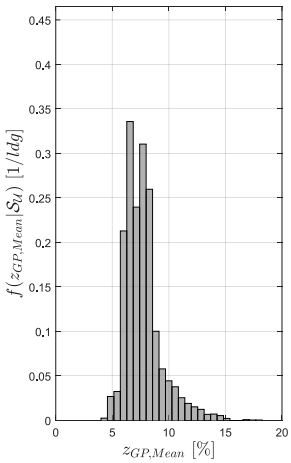

Figure 27: Distribution- $z_{GP,Mean}$

7. Conclusion

The requirements and details of the automatic landing procedure for HAPS A/C aircraft with a large aspect ratio and low wing loading have been described. The design of the Autoland function based on the concept of TECS, incorporating thrust for total energy control and elevator for speed and flight path control, is outlined in the paper. To enable the three-point landing of the taildragger A/C, the control allocation is adapted over the runway. In contrast to

DOI: 10.13009/EUCASS2023-949

the classical TECS, the flaps are continuously used for vertical speed control. In addition to the TECS description, the integration of the proposed adaptions into a common cascaded control architecture built around a TECS is described. An extensive Monte Carlo simulation was conducted to perform the risk analysis for verifying the reliability and robustness of the Autoland function. The FCL has been shown to fulfil the requirements concerning the landing zone, and precision of airspeed and glide path tracking. However, it should be noted that the system falls short of ensuring a touchdown within the specified limits for vertical speed and maximum forces on the main landing gear. This issue seems to result from large vertical turbulence below 10 m above ground that the CS-AWO turbulence model generates. While the CS-AWO turbulence model has proven adequate for CS-25 transport category A/C, its vertical turbulence components may be unrealistic close to the ground, i.e. below 10 m above the ground - as the vertical component must be zero at $H_{GND} = 0$ m. The suitability of the turbulence model for A/C with low wing loading requires further validation and its adaption towards A/C with low wing loading may be necessary.

Acknowledgements

The presented work is the result of the FCL-HALE research project at the Department for Flight Mechanics, Flight Control and Aeroelasticity, Technische Universität Berlin. FCL-HALE was funded and supervised by Leichtwerk AG. The results and methods were refined in the scope of the subsequent joint project IBAS in the context of the public sponsorship program Niedersächsische Luftfahrtförderrichtlinie funded by NBank.

References

[1] EASA. 2022: Easy Access Rules for Unmanned Aircraft Systems. Regulation (EU) 2019/947 and Regulation (EU) 2019/945. September 2022.
[2] EASA. 2022: Certification Specifications and Acceptable Means of Compliance for All-weather Operations (CS-AWO). Issue 2, Cologne: January 2022.
[3] EUROCAE. 2021: MASPS for RPAS Automatic Take-off and Landing (ATOL). ED-283, Issue 1, Saint-Denis, France: February 2021.
[4] ICAO. 2018: Procedures for Air Navigation Services - Aircraft Operations (PANS-OPS). ICAO DOC 8168, Sixth Edition. Montreal, Canada: 2018.
[5] Lambregts, A. A. 1983: Vertical flight path and speed control autopilot design using total energy principles. In: *Proceedings of the AIAA Guidance and Control Conference* 1983, No. AIAA 83-2239, Gatlinburg,TN.
[6] Lambregts, A. A. 1984: Total Energy Based Flight Control System. Pat.WO 84/01345.
[7] Lambregts, A. A. 2013: TECS Generalized Airplane Control System Design – An Update. In: *Advances in Aerospace Guidance, Navigation and Control*. 503-534. Springer Berlin Heidelberg.
[8] Bruce, K. R.: NASA B737 Flight Test Results of the Total Energy Control System. Final Report NASA CR-178285. NASA.
[9] Brockhaus, R., W. Alles, and R. Luckner. 2011: Flugregelung. 3. Auflage. Springer, Berlin, Heidelberg.
[10] Lamp, M. 2015: Automatische, schublose Landung eines Flugzeuges großer Streckung unter Verwendung der Bremsklappen und mit variablen Gleitpfadwinkeln. Dissertation. TU Berlin.
[11] Lamp, M., and R. Luckner. 2013: The Total Energy Control Concept for a Motor Glider. In: *Advances in Aerospace Guidance, Navigation and Control*. 483–502. Springer, Berlin, Heidelberg.
[12] Lamp, M., and R. Luckner. 2015: Automatic Landing of a High-Aspect-Ratio Aircraft without Using the Thrust. In: *Advances in Aerospace Guidance, Navigation and Control*. 549-567. Springer, Cham.
[13] Kastner, N., and G. Looye. 2013. Generic TECS based autopilot for an electric high altitude solar powered aircraft. In: *Proceedings of the EuroGNC 2013*, Delft.
[14] Weiser, C., and D. Ossmann. 2022. Baseline Flight Control System for High Altitude Long Endurance Aircraft.
[15] Hasan, Y.J., M.S. Roeser, M. Hepperle et al. 2023: Flight mechanical analysis of a solar-powered high-altitude platform. In: *CEAS Aeronautical Journal*, vol. 14. 201–223.
[16] Joos, H.D. 1997: Multi-objective parameter synthesis (MOPS). In: *Robust Flight Control. Lecture Notes in Control and Information Sciences*, vol 224. Springer, Berlin, Heidelberg.
[17] Chernetsov, D., B. Laabs, R. Paul, and R. Luckner. 2023: Model-Based Development of a Library with Standard Functions for Safety-Critical Flight Control Laws. In: *Proceedings of the EUCASS-CEAS Conf. 2023*, Lausanne.
[18] Lambregts, A. A. 1982: Avoiding the pitfalls in automatic landing control system design. In: *AIAA Guidance and Control Conference*.
[19] Kickert, R. 2021: High Altitude Platform Stations (HAPS). In: *Magazin Luft- und Raumfahrt*, Heft 2/2021. 17-19. Bonn.
[20] StratoRPAS GmbH: Solutions and Technology. URL: https://haps-broadband.org/wp-content/uploads/2021/03/Bild_5_HAPS-StratoStreamer-768x388.jpg, last visit 04.07.2023.